Inorganic Chemistry

Open Access
This article is licensed under CC-BY 4.0

pubs.acs.org/IC
Article

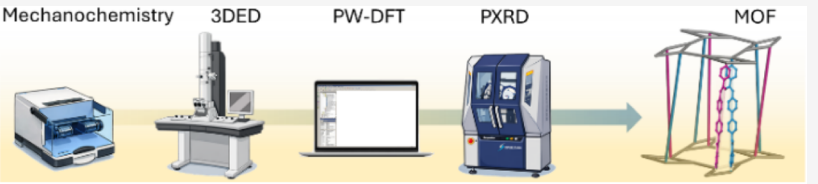
Mechanochemistry-Accessed MOF Polymorphism Revealed by an Integrated 3DED/DFT-Assisted Rietveld Analysis

Giorgio Cagossi, Andrea Daolio, Dario Giovanardi, Iryna Andrusenko, Enrico Mugnaioli, Lucia Carlucci, Paolo P. Mazzeo,* Alessia Bacchi, and Paolo Pelagatti*

Cite This: *Inorg. Chem.* 2026, 65, 18639−18647

Read Online

ACCESS | Metrics & More | Article Recommendations | Supporting Information



ABSTRACT: A combined 3DED, plane-wave DFT, and Rietveld refinement workflow uncovers the first example of interlayer-twisting polymorphism in a pillared MOF. While the parent material, **PUM198**, a Zn-based mixed-ligand MOF, was previously synthesized under solvothermal conditions, mechanochemistry selectively affords a new polymorph, **PUM198-m**. Although the two phases share identical composition and connectivity, they differ in symmetry, layer arrangement, pore architecture, and topology. Accessible only as a microcrystalline powder, **PUM198-m** is unsuitable for conventional single-crystal X-ray diffraction, and its flexibility and solvent-filled pores preclude structure solution from the XRPD data. The crystal structure was therefore derived from a multitechnique blueprint in which the starting model was derived from 3DED data and subsequently refined through iterative DFT-assisted Rietveld analysis to describe the as-synthesized, guest-loaded material. This integrated workflow provides a broadly applicable structural elucidation strategy for flexible MOFs that are mechanochemically synthesized, for which conventional crystallographic analysis fails.

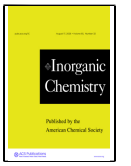
INTRODUCTION

Mechanochemistry has emerged as a powerful synthetic strategy in which chemical transformations are driven by mechanical energy, typically through the grinding of solid reactants.[1] By minimizing or eliminating solvent use, this approach reduces the environmental impact, improves reaction efficiency, and lowers production costs. Beyond its sustainability advantages, mechanochemistry can also unlock reaction pathways that are inaccessible or inefficient under conventional solution-based conditions.[1−4]

Metal−organic frameworks (MOFs) represent a prominent class of porous crystalline materials composed of metal-containing secondary building units (SBUs) interconnected by organic linkers.[5−7] Their structural diversity and tunable porosity underpin applications in gas storage, separation, catalysis, and sensing.[8−13] The transformative impact of MOF chemistry was recently recognized by the 2025 Nobel Prize in Chemistry, awarded to Kitagawa, Yaghi, and Robson for their pioneering contributions to the field.[14] A wide range of archetypal MOFs, primarily synthesized via wet chemistry, have now been successfully reproduced by mechanochemical protocols, including copper(II) isonicotinate,[15] HKUST-1,[16] MOF-5,[17] UiO-66,[18] and several zeolitic imidazolate frameworks (ZIFs),[19−21] with no compromise in terms of crystallinity with respect to their solvothermal counterparts.

Among MOFs, those with a pillared-layered architecture (PL-MOFs) occupy a particularly versatile niche. These materials consist of two-dimensional metal-carboxylate layers interconnected by N-containing axial pillars,[22] like bis-pyridines, bis-amines, bis-imidazoles, or pyrazines, thus combining two chemically distinct linker types within a single framework. This modular design enables extensive functionalization and structural tunability.[23−26] The successful mechanochemical preparation of PL-MOFs such as $[Zn_2(5\text{-aip})_2(bipy)]$[27] (5-aip = 5-aminoisophthalate, bipy = 4,4′-bipyridine), reflects the growing recognition that mechanochemical strategies can be even applied to increasingly complex framework architectures. Moreover, we have recently achieved the dimensionality growth of 1D-coordination polymers containing dpe (dpe = 1,2-bis(4-pyridyl)ethylene) to 3D PL-MOFs via insertion of terephthalate under mechanochemical conditions.[28] Previously, our group developed, under solvothermal conditions, a new family of PL-MOFs named PUM

Received: April 22, 2026
Revised: July 29, 2026
Accepted: July 31, 2026
Published: August 6, 2026



Downloaded from pubs.acs.org/inocaj/article-pdf/65/32/18639/6435106/acs.inorgchem.6c02037.pdf by UNIV DEGLI STUDI DI PARMA user on 08 September 2026

ACS Publications
© 2026 The Authors. Published by American Chemical Society

https://doi.org/10.1021/acs.inorgchem.6c02037
Inorg. Chem. 2026, 65, 18639−18647

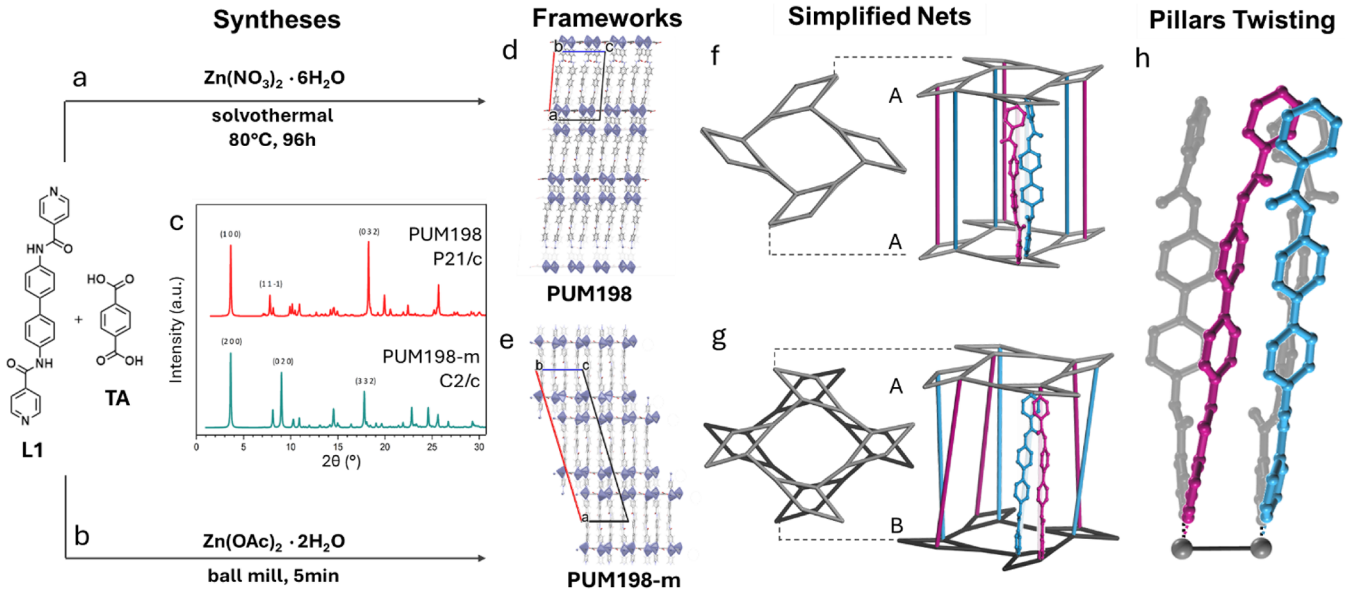


Figure 1. (a) Synthesis details for **PUM198** (solvothermal) and (b) **PUM198-m** (ball-milling) with a scheme of the ligands used. (c) Calculated PXRD patterns of **PUM198** (red line) and **PUM198-m** (green line) with represented plane families highlighted. (d) Framework visualizations of **PUM198** (Refcode: ZILDEG[30]) and (e) **PUM198-m** with Zn atoms depicted in polyhedral style and nonmetal atoms depicted as sticks. H atoms and guest molecules are removed for the sake of clarity. Double interpenetration is highlighted by representing the second framework in transparency. Unit cells are reported to emphasize the *P*-centered (**PUM198**) against the *C*-centered (**PUM198-m**) structure. (f) Simplified nets of **PUM198** and (g) **PUM198-m** highlighting the rotation of the 2D-squared layers containing TA^{2-} anions with consequent pillar twisting. (h) Pillars twisting in **PUM198-m** highlighted by superimposition of two adjacent **L1** ligands (colored) with the same ligands in **PUM198** (gray transparency). Zn atoms, reported as gray balls, are superimposed to stress the pillar orientation differences.

(Parma University Materials). These MOFs contain a series of extended bis-amidic pillars,[29] in which amide groups serve as hydrogen-bond donors and acceptors, creating internal recognition sites for supramolecular interactions. Such features enhance affinity toward a wide range of guest molecules, including natural phenolic terpenoids[30−32] and nitrogen-containing heterocycles,[33] leading to controlled guest release. Among the PUM family,[34] **PUM198**, made of terephthalate spacers and rigid bis-pyridine-bis-amide pillars (**L1**, Figure 1), was revealed to be ideal for adsorbing polyaromatic heterocycles through noncovalent interactions.[35] Based on the potential applications offered by PUM materials, the development of a mechanochemical synthetic route is highly desirable to overcome the typical limitations of solvothermal synthesis. Herein, we explored the mechanochemical synthesis of the previously reported solvothermal synthesis of **PUM198**, consistently and selectively yielding a different polymorphic form, **PUM198-m** (Figure 1). When prepared via mechanochemistry, the material is produced as a microcrystalline powder, precluding structure determination by conventional single-crystal X-ray diffraction (SCXRD). Three-dimensional electron diffraction (3DED) data collection performed in TEM on individual submicrocrystals directly harvested from the milling jar allows for complete structural elucidation, overcoming the intrinsic limitations associated with nonrecrystallizable materials. Efficiency and accuracy of the structure solution and refinement are increased when data are collected in association with beam precession[36] and/or with continuous sample rotation (cRED).[37,38] Recently, the possibility of applying serial electron diffraction (SerialED) on MOFs has also been explored.[39] The combination of mechanochemical synthesis and electron crystallography therefore represents a broadly applicable and transformative strategy for the routine structural characterization of nano- and microcrystalline framework materials.[40−42]

Polymorphism in MOFs is well-documented,[43−48] yet cases where distinct synthetic routes produce polymorphs through subtle framework-level conformational reorganization remain uncommon.[49] In most cases, structural variations arise from linker flexibility,[50] changes in SBU geometry or connectivity,[51,52] or kinetic trapping of alternative node assemblies.[53] Although linker design has been shown to guide framework connectivity,[54] polymorphism originating from different spatial orientations of the same rigid linker under distinct synthetic protocols is a rare condition.

PL-MOFs, such as **PUM198**, are known to exhibit pronounced structural flexibility, often undergoing substantial lattice distortions upon guest inclusion or removal.[30,31,33] Such breathing behavior can involve changes in interlayer spacing, pore geometry, and even symmetry or unit-cell metrics. Host−guest interactions are typically governed by weak, noncovalent forces, so the incorporated solvent molecules can be readily evacuated under mild vacuum conditions, frequently inducing framework rearrangements.[55] Such responsiveness complicates structural characterization, as 3DED data collected in a high vacuum environment may not directly reflect the as-synthesized, solvent-loaded state of the material.

Here, we introduce a robust and transferable multitechnique workflow that integrates electron diffraction, Plane Wave-Density Functional Theory (PW-DFT) calculations, and Rietveld refinement into a unified structure-solution strategy that may serve as a blueprint for the structural elucidation of mechanochemically derived microcrystalline frameworks. The framework model obtained from 3DED served as the starting platform for iterative DFT-assisted Rietveld refinement, allowing the correct structural incorporation of dimethylformamide (DMF) guest molecules into the crystallographic

https://doi.org/10.1021/acs.inorgchem.6c02037
Inorg. Chem. 2026, 65, 18639−18647

Downloaded from pubs.acs.org/inocaj/article-pdf/65/32/18639/6643510/acs.inorgchem.6c02037.pdf by UNIV DEGLI STUDI DI PARMA user on 08 September 2026

model. The guest content was quantified by Nuclear Magnetic Resonance (NMR) spectroscopy and by thermogravimetric analysis (TGA), ultimately yielding a fully resolved and experimentally validated crystal structure of **PUM198-m** and granting access to its "as-synthesized" framework.

EXPERIMENTAL AND COMPUTATIONAL SECTION

Materials and Methods

All reagents and solvents were of high purity and used as received, unless otherwise indicated. *N*,*N*-Dimethylformamide (99.9% purity) was purchased from Carlo Erba. Ligand **L1** was synthesized according to a previously described procedure.[29]

Synthesis

All mechanochemical syntheses were performed in a Retsch MM400 mixer mill, utilizing 5 mL stainless steel jars and balls of the same material (Ø = 10 mm, $w \approx 4$ g). Liquid-Assisted Grinding (LAG) conditions were applied, using a small volume of DMF. In the following, the symbol η refers to the ratio between the volume of DMF (μL) and the mass of solids (mg). $Zn(OAc)_2{\cdot}2H_2O$ (55 mg, 0.25 mmol), **L1** (98 mg, 0.25 mmol), terephthalic acid (42 mg, 0.25 mmol), and DMF (200 μL, η = 0.66 μL/mg) were introduced into the jar along with one ball. The jar was shaken for 5 min at 30 Hz. The product was retrieved, washed three times with DMF (1 mL), and dried in air to obtain a yellow powder. Yield: 91% (based on Zn content).

Powder X-ray Diffraction

PXRD data for phase checking and quantification were collected in the Bragg–Brentano geometry with Cu Kα radiation on a Rigaku SmartLab XE diffractometer equipped with a solid-state HyPix-3000 2D detector. The samples were placed on a glass sample holder and measured with a scan rate of 5° min^{-1} in the range $1.5° \leq 2\theta \leq 50°$. Every sample was vertically aligned with respect to the incoming beam to moderate the vertical sample displacement. A length-limiting slit of 10 mm was used as a compromise to enhance X-ray flux over the sample, while 2.5° Soller slits improved the peak profile and reduced reflection overlap. Data collection for Rietveld Refinement was performed in Debye–Scherrer geometry with the sample loaded in a sealed borosilicate glass capillary (Ø 0.3 mm, 80 mm length) mounted on the capillary spinner and measured under continuous rotation (2 Hz) to minimize preferred orientation effects. PXRD data analyses were performed with TOPAS V6.[56] Pawley refinement was performed considering a seventh-order Chebyshev polynomial function to fit the background and a TCHZ function for the definition of the line profile (Figures S6–S7). The same input layout was also used for the Rietveld Refinement (Figures S8–S9) with the structure obtained from DFT optimization included as a rigid body with rotation and translation free to vary within a limited constrained range (±10°) in the first refinement. Once refined, rotation and translation of the rigid body were kept fixed, while intramolecular rotations of the ligands were refined, although constrained within a limited range (±10°). After the framework optimization, DMF positions were refined by the constrained H-bond lengths and angles with a tolerance of 10%. All atoms were isotropically refined.

TEM and Three-Dimensional Electron Diffraction

A small tip of powdered sample (less than 1 mg) was gently ground between two glass plates and then sprinkled on a carbon-coated Cu TEM grid. The sample was analyzed with a JEOL JEM F200 Multipurpose TEM, working at 200 kV and equipped with a Schottky field emission gun (FEG). The pressure inside the column was about 2×10^{-5} Pa, a high vacuum guaranteed by a dedicated superionic pump with a capacity of 150 L/s. 3DED was performed in scanning transmission electron microscopy (STEM) mode after defocusing the beam in order to achieve pseudoparallel illumination on the sample.[57,58] 3DED data were collected with a beam size of about 30 nm in diameter, obtained using a 10 μm C2 condenser aperture and the highest probe size (10). Data collections were performed in stepwise mode (tilt step = 1°), and the covered tilt ranged up to 100°. After each tilt, a diffraction pattern was acquired, and the crystal position was tracked by defocused STEM imaging, performed with high-angle annular dark-field (HAADF-STEM). The camera length was set to 300 mm, allowing for a resolution in real space of about 1.0 Å. The beam was precessed around the optical axis by an angle of 1° to properly integrate every reflection over the excitation error.[59] Precession was obtained using a Nanomegas Digistar P1000 device. 3DED data were recorded by an ASI CheeTah hybrid-pixel electron detector (512 × 512 pixels) and analyzed with the program PETS2.0.[60] The structure solution was performed in two steps. Inorganic clusters were solved ab initio by standard direct methods (SDM), while position and conformation of organic linker molecules were determined by simulated annealing (SA). Both methods are implemented in the SIR2014 software package.[61] The molecules of terephthalate and bis-pyridine–bis-amide were extracted from the solvothermal **PUM198** structure (Refcode: ZILDEG). This method has been previously applied for the determination of covalent organic frameworks,[62] hybrid perovskites,[63] and important pharmaceuticals.[64,65] The achieved structural data were refined with a fully kinematical approximation, i.e., neglecting dynamical scattering and assuming that I_{hkl} is proportional to $|F_{hkl}|^2$.

PW-DFT Calculation Details

Starting from the 3DED-determined atomic positions with the addition of 5 DMF molecules (manually added with the Materials Studio program[66] to mimic the position of guest molecules in the parent solvothermal **PUM198** structure), the structure was optimized by means of the *PW*-DFT program CASTEP 2023.1.[67] The choice of parameters employed in the geometry optimization was tailored to provide a general scheme applicable to the DFT-Assisted Rietveld refinement of MOFs while optimizing for computational resources and is in line with other works on the subject.[68−70] The wave function was expanded in plane waves to a kinetic energy cutoff of 400 eV. The electronic structure was sampled at the Γ point. The exchange-correlation functional of Perdew–Burke–Ernzerhof (PBE)[71] was used with the dispersion correction of Tkatchenko–Scheffler (TS).[72] The core–valence interaction was modeled with a norm-conserving pseudopotential generated on-the-fly as implemented in CASTEP. Convergence was accepted when residual atomic forces reached $<1 \times 10^{-2}$ eV $Å^{-1}$, with SCF convergence accepted at $<1 \times 10^{-6}$ eV. The Pulay density mixing scheme was employed as the electronic minimizer algorithm. The DFT optimizations had the unit cell restrained to the PXRD-indexed cell parameters, while all the atomic positions could be optimized.

Thermogravimetric Analysis

TGA analyses were performed with a PerkinElmer TGA 8000 instrument (mass sample: 1–3 mg) by means of a Pt crucible under an air flux (30 mL/min) in the temperature range of 30–500 °C at 10 °C/min. Higher temperatures were not applied to avoid possible crucible damage due to the high metal content of the samples.

^{1}H NMR Spectroscopy

^{1}H NMR spectra were recorded on a Bruker Avance spectrometer operating at 400 MHz at 25 °C after dissolving the sample in CF_3COOD (TFA-d) and diluting it with $(CD_3)_2SO$ (DMSO-d_6). Chemical shifts (δ) are expressed in ppm relative to the residual peak of deuterated DMSO (^{1}H = 2.50 ppm).

Semiquantitative ^{1}H NMR analyses were performed to estimate the relative amount of coordinated and/or included DMF with respect to the MOF. After complete dissolution of the sample, the integrals were referenced to well-resolved, nonoverlapping proton signals of the two organic ligands, which were considered together as one asymmetric unit. The characteristic singlet of DMF (N–CH_3) at ca. δ = 7.95 ppm was integrated and compared with pyridinic C–H proton resonances of the ligands at ca. δ = 9.1 ppm. The integrals were normalized according to the number of protons contributing to each signal, allowing determination of the molar ratio between DMF and the asymmetric unit.

Downloaded from pubs.acs.org/inocaj/article-pdf/65/32/18639/6435106/acs.inorgchem.6c02037.pdf by UNIV DEGLI STUDI DI PARMA user on 08 September 2026

https://doi.org/10.1021/acs.inorgchem.6c02037
Inorg. Chem. 2026, 65, 18639−18647

Topological Analysis

The topological analysis of **PUM198-m** and **PUM198** was performed using ToposPro software, applying the standard simplification procedure.[73] The search for structures exhibiting the same topological type and degree of interpenetration as **PUM198-m** was carried out by accessing the TopCryst database through the website resource (https://topcryst.com/).[74]

BET Measurements

Adsorption measurements were carried out using a BELSORP MAX X porosimeter employing N_2 5.0 gas. BET was estimated using BELmaster software in the P/P_0 range of 0.01−0.1 bar.

Crystallographic Details

RESULTS AND DISCUSSION

Synthesis

PUM198 is a PL-MOF made of Zn(II) nodes coordinated by terephthalate ($\mathbf{TA}^{2-}$) linkers and the bis-pyridine−bis-amide pillar **L1.** The resulting framework is built around a double-pillared bimetallic SBU of formula $[Zn_2(\mu\text{-}COO)_2(\kappa^1\text{-}COO)_2(py)_4]$, where the two carboxylate groups of each $\mathbf{TA}^{2-}$ anion behave differently. These units arrange together into two-dimensional layers, subsequently pillared by the axial bis-amidic ligands, generating the three-dimensional framework (Figure 1a).

The original solvothermal synthesis employed zinc nitrate hexahydrate as the metal source (Figure 1a). Direct transfer of these conditions to mechanochemical synthesis using DMF as a LAG additive (30 Hz, one 10 mm Ø SS ball) was unsuccessful. Addition of a base (a stoichiometric amount of triethylamine corresponding to the complete neutralization of **TA**) after 5 min of milling resulted in the formation of multiple phases but not the desired **PUM198-m**. Replacing zinc nitrate with the more basic zinc acetate dihydrate proved crucial for successful mechanochemical synthesis (Figure 1b). Under solvothermal conditions, DMF can partially decompose into basic species such as dimethylamine, which promotes the slow deprotonation of the dicarboxylic linker and enables MOF formation from $Zn(NO_3)_2{\cdot}6H_2O$. In contrast, under mechanochemical conditions, this source of in situ basicity is absent, making the more basic $Zn(OAc)_2{\cdot}2H_2O$ ideal to facilitate linker deprotonation and framework assembly.[75] The optimized procedure involved loading zinc acetate together with both ligands in a 1:1:1 stoichiometric ratio (Zn^{2+}:**TA**:**L1**) and addition of a small volume of DMF. Remarkably, complete conversion to **PUM198-m** as the sole crystalline phase was achieved within 5 min, affording a bright yellow dry powder with high yield (91% after washing and air drying). Milling times beyond 5 min did not improve the yield, although the material demonstrated good mechanical stability and crystallinity, even after prolonged milling time (several hours, see Supporting Information and Figures S11−S12). The LAG ratio of η = 0.66 μL/mg proved optimal, whereas values lower than 0.50 were unsuccessful, leading to mixtures of phases. Importantly, strict adherence to the 1:1:1 stoichiometric ratio was essential to obtain **PUM198-m** as a single phase, as deviation from this ratio led to the formation of secondary undefined crystalline phases. This stoichiometric requirement reflects the 1:1:1 metal-to-ligand composition of the **PUM198-m** framework.

PUM198-m Structural Determination

3D ED-TEM. Independent 3DED data sets were collected from several crystalline fragments smaller than 1 μm (Figure 3b). All data sets exhibited the systematic extinction condition *h*0*l*: *l* = 2*n*, consistent with a *C*-centered monoclinic lattice. The data set covering the largest tilt range and free of artifacts arising from polycrystallinity was selected for structure determination. The refined unit-cell parameters were approximately *a* = 48.3(2), *b* = 19.7(2), *c* = 15.2(4) Å, with β = 97.4(3)°. Structure solution was achieved in the centrosymmetric space group *C*2/*c*.

The mechanochemically obtained framework retains the same connectivity as the solvothermal analogue **PUM198** (Figure 1d−g). A small variation involves the SBU that now has the formula $[Zn_2(\mu\text{-}COO)_2(\kappa^1\text{-}COO)(\kappa^2\text{-}COO)(\mathbf{L1})_4]$, where the two nonbridging carboxylates behave differently, one being κ^1-monodentate and the other being κ^2-chelating (Figure S1). However, differences in linker orientation induce a displacement and rotation of adjacent layers in **PUM198-m** (Figure 1f−g), resulting in a symmetry change from $P2_1/c$ (**PUM198**) to *C*2/*c* (Table 1), with a consequent doubling of the cell volume and *a*-axis. In **PUM198**, the bis-amidic pillars are parallel and generate a regular A−A−A stacking sequence of the orthogonal zinc-carboxylate 2D layers. In contrast, in **PUM198-m**, the two pillars adopt a twisted arrangement, coiling around one another by approximately 90°, thereby connecting orthogonal squared layers rotated by 90° relative to each other, producing an A−B−A−B stacking pattern consistent with the *C*-centered symmetry (Figure 1). Like its parent phase, **PUM198-m** exhibits 2-fold interpenetration of class IIa (i.e., the two frameworks are related by a center of inversion) (Figure S4), with both nets being binodal 3,5-connected. The differences lie in the topology of the 3,5-c nets, particularly in the point symbols of the 3-c nodes, which are (4.6^2) in **PUM198** and (4.6.8) in **PUM198-m**, corresponding to the **fet** and **fsc**-3,5-*Ibam* topologies, respectively (Figure S15).[76] A search of the TopCryst database[74] for 2-fold

Table 1. Crystallographic Details for PUM198-m as Refined by Rietveld Refinement

	PUM198-m
CCDC Deposition Number	2541762
Phase Percentage	100%
Chemical Formula	$C_{64}H_{44}N_8O_{12}Zn_2{\cdot}5(C_3H_7NO)$
Formula Weight	1552.6616
Z	8
Temperature (K)	298(2)
Space Group	*C*2/*c*
a (Å)	50.9649(2)
b (Å)	19.6008(3)
c (Å)	15.5652(3)
β (°)	107.4035(6)
V (Å^3)	14837.1(4)
ρ (g/cm^3)	1.444
Rbragg (%)	4.04
Rp (%)	6.78
Rwp (%)	8.76
Refinement Method	Rietveld
Measurement Device Type	Rigaku Smartlab XE
Radiation Wavelength (Å)	1.5406
Measurement Method	Continuous Scan

Downloaded from pubs.acs.org/inocaj/article-pdf/65/32/18639/6435106/acs.inorgchem.6c02037.pdf by UNIV DEGLI STUDI DI PARMA user on 08 September 2026

https://doi.org/10.1021/acs.inorgchem.6c02037
Inorg. Chem. 2026, 65, 18639−18647

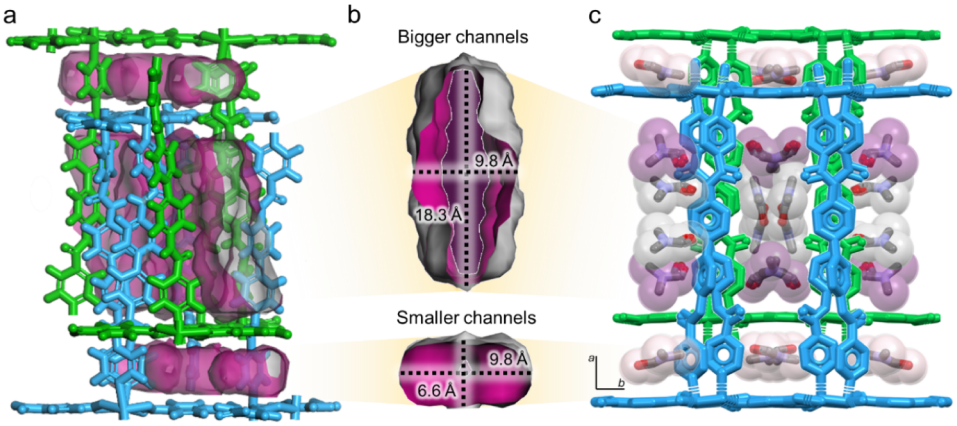


Figure 2. (a) Porosity of **PUM198-m**. Interpenetrated nets are highlighted with different colors. Channel surfaces are highlighted in purple. (b) Channel voids along the *c*-axis with superimposed pore dimensions. (c) Detail of the DMF molecules hosted within the framework along the *c*-axis: symmetry-related molecules are haloed with the same color.

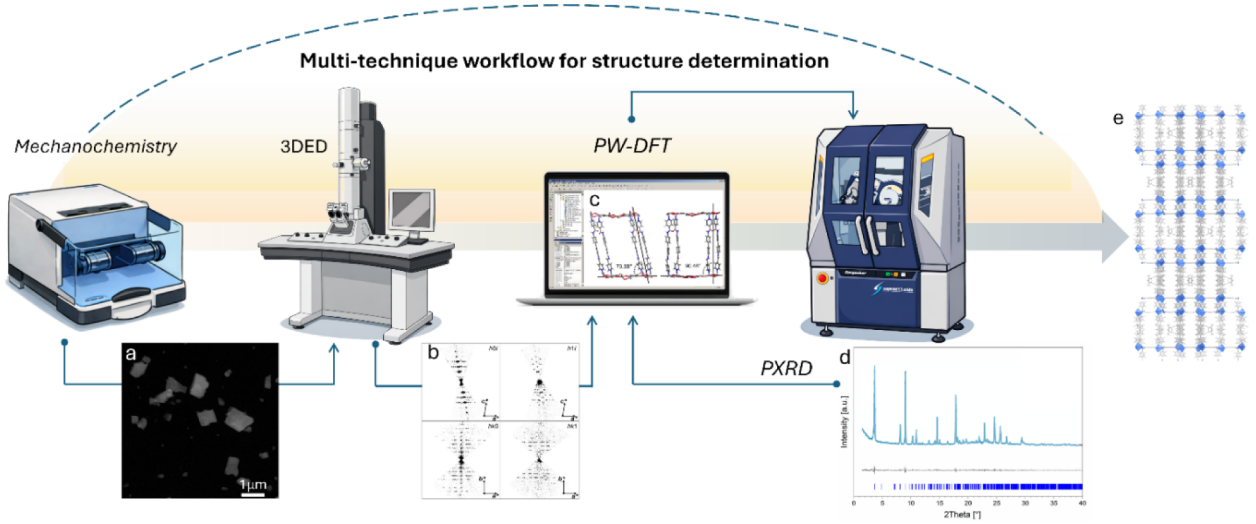


Figure 3. Schematic workflow followed for the structural elucidation of **PUM198-m**. The sample was directly obtained from mechanochemistry as microcrystalline powder (a), which was directly measured by 3D ED-TEM (b). The cell parameters were first refined against PXRD experimental data collected on the freshly synthesized sample, then the initial model structure with the addition of DMF molecules was minimized by the PW-DFT algorithm (c) and finally Rietveld refined against the PXRD experimental pattern (d), thus leading to the final model of **PUM198-m** (e).

interpenetrated structures with the **fsc**-3,5-*Ibam* topology returned only three PL-MOF structures (refcodes: BOWSIQ, EWESAC, and QOYZUD), whose topological analysis revealed a twisting of the metal−carboxylate layers similar to that observed in **PUM198-m**.[77]

The framework defines two distinct rectangular channels running along the *c*-axis (Figure 2a). The larger channels display window dimensions of approximately 18.3 × 9.8 Å^2, whereas the smaller one measures about 6.6 × 9.8 Å^2 (Figure 2b). The calculated void volume (32%) closely matches that of **PUM198** (31%), indicating that interlayer twisting preserves the overall porosity. The experimentally measured BET surface areas of the activated materials indicate an increase for **PUM198-m**, from 46 to 75 m^2/g (see Supporting Information and Figures S16), although the absolute values remain rather low for both materials. Nevertheless, the reorientation of the linkers alters the amide exposure within the channels (Figure 1h).

Although structural modifications arising from subtle twisting and/or sliding motions in interpenetrated frames have been reported,[78] polymorphism arising from plane twisting in PL-MOFs is unprecedented and markedly different from the more commonly reported structural variants originating from pillar flexibility.[79]

While the 3DED-derived model unambiguously establishes the framework connectivity and topology, it does not resolve the positions of the native DMF guest molecules, which may have an impact on the whole framework arrangement. Their presence within the pores of the mechanochemically synthesized product was confirmed by ^{1}H NMR spectroscopy (Figure S13) and TGA analysis (Figure S14). The absence of electron density corresponding to DMF likely results from the high-vacuum conditions inherent to electron diffraction, which promote solvent evacuation during data acquisition and induce the associated framework distortion.

DFT-Assisted Rietveld Refinement

PXRD data were collected on freshly mechanochemically synthesized **PUM198-m,** loaded in a 0.3 mm Ø glass capillary with high-resolution Soller slits to improve angular resolution. Initial indexing using the unit cell parameters derived by 3D ED-TEM returned only a modest agreement with the

Downloaded from pubs.acs.org/inocaj/article-pdf/65/32/18639/6643510 6/acs.inorgchem.6c02037.pdf by UNIV DEGLI STUDI DI PARMA user on 08 September 2026

https://doi.org/10.1021/acs.inorgchem.6c02037
Inorg. Chem. 2026, 65, 18639−18647

experimental pattern (Rwp 23.85), symptomatic of substantial framework distortion upon solvent removal from the pores due to the electron diffraction setup. The set of unit cell parameters was validated by Pawley refinement (*C*2/*c*; *a* 50.98(2), *b* 19.60(3), *c* 15.57(2) Å, *β* 107.42(2)°), with a significantly improved match against the experimental data (Rwp 5.19) (Figures S2, S6–S7).

The structural model with the atomic positions determined from 3DED was used as a starting platform for the DFT optimization (CASTEP[67]) with the inclusion of five DMF molecules *per* asymmetric unit, as determined by ^{1}H NMR and TGA. The amount of guest molecules added is compatible with the volume of DMF that was inserted into the jar. The DMF molecules were initially positioned into the **PUM198-m** pores, mimicking those found in the parent **PUM198**. During the DFT optimization, the unit-cell parameters were fixed to the PXRD-indexed values, while all atomic positions were allowed to relax (see the Experimental and Computational Section for details).

Rietveld refinement was finally performed against the PXRD data using the DFT-optimized structure. The framework was treated as a rigid body in TOPAS[56] with fixed bond lengths and angles, while limited conformational flexibility (≤10°) was allowed to account for internal ligand relaxation and rotation about coordination axes. Coordination bond lengths were further refined to account for thermal effects. Finally, the positions of the DMF molecules were optimized, allowing for the refinement of the hydrogen bond distances and angles, as evidenced in Figure 2c (see also Figure S5).

After DFT optimization and Rietveld refinement (Figures S8–S9, the final structural model of **PUM198-m** was found to closely match the original as-synthesized **PUM198-m** structure. The high degree of agreement between the experimental PXRD pattern and those simulated from the different structural models further supports this conclusion (as shown in Figures S3, S10, S17, and S18).

A schematic workflow followed for the structural elucidation of **PUM198-m** is shown in Figure 3.

CONCLUSIONS

The integration of three-dimensional electron diffraction with DFT-assisted Rietveld refinement constitutes a robust and broadly applicable strategy for the structural elucidation of mechanochemically derived nano- and microcrystalline frameworks. By combining reciprocal-space information from 3DED with computationally guided refinement of powder diffraction data, this workflow overcomes the intrinsic limitations of single-crystal diffraction and enables reliable modeling of flexible, guest-containing materials. Beyond resolving the structure of **PUM198-m**, this multitechnique approach establishes a transferable blueprint for characterizing complex framework materials that cannot be recrystallized. Importantly, its application here reveals a previously unknown polymorph arising from a subtle reorientation of rigid pillars, which induces interlayer twisting and symmetry modulation without altering the overall connectivity or composition, a type of structural variation not reported for PL-MOFs. This finding highlights how mechanochemistry can selectively access alternative structural states encoded within a given framework, uncovering latent degrees of freedom in MOF architectures and expanding the structural landscape accessible to porous materials.

ASSOCIATED CONTENT

Supporting Information

The Supporting Information is available free of charge at https://pubs.acs.org/doi/10.1021/acs.inorgchem.6c02037.

Experimental, crystallographic, X-ray traces, and computational details, mechanical stability, ^{1}H NMR spectrum, TGA trace of**PUM198-m**, and BET traces of **PUM198** and **PUM198-m** (PDF)

Accession Codes

Deposition Number 2541762 contains the supplementary crystallographic data for this paper. These data can be obtained free of charge via the joint Cambridge Crystallographic Data Centre (CCDC) and Fachinformationszentrum Karlsruhe Access Structures service.

AUTHOR INFORMATION

Corresponding Authors

Paolo Pelagatti − *Department of Chemical Sciences, Life Science and Environmental Sustainability, University of Parma, Parma 43124, Italy; Interuniversity Consortium of Chemical Reactivity and Catalysis (C.I.R.C.C.), Bari 70126, Italy;* orcid.org/0000-0002-6926-2928; Email: paolo.pelagatti@unipr.it

Paolo P. Mazzeo − *Department of Chemical Sciences, Life Science and Environmental Sustainability, University of Parma, Parma 43124, Italy; Biopharmanet-TEC, University of Parma, Parma 43124, Italy;* orcid.org/0000-0002-5787-3609; Email: paolopio.mazzeo@unipr.it

Authors

Giorgio Cagossi − *Department of Chemical Sciences, Life Science and Environmental Sustainability, University of Parma, Parma 43124, Italy;* orcid.org/0009-0005-6356-609X

Andrea Daolio − *Department of Chemical Sciences, Life Science and Environmental Sustainability, University of Parma, Parma 43124, Italy;* Present Address: Andrea Daolio, Department of Chemistry, Stockholm University, Svante Arrhenius väg 16C, Stockholm, Sweden, SE-106 91

Dario Giovanardi − *Department of Chemical Sciences, Life Science and Environmental Sustainability, University of Parma, Parma 43124, Italy*

Iryna Andrusenko − *Centre for Instrumentation Sharing of the University of Pisa (CISUP), University of Pisa, Pisa 56426, Italy*

Enrico Mugnaioli − *Centre for Instrumentation Sharing of the University of Pisa (CISUP), University of Pisa, Pisa 56426, Italy; Department of Earth Sciences, University of Pisa, Pisa 56126, Italy;* orcid.org/0000-0001-9543-9064

Lucia Carlucci − *Department of Chemistry, Università Degli Studi di Milano, Milano 20133, Italy;* orcid.org/0000-0001-5856-5280

Alessia Bacchi − *Department of Chemical Sciences, Life Science and Environmental Sustainability, University of Parma, Parma 43124, Italy; Biopharmanet-TEC, University of Parma, Parma 43124, Italy;* orcid.org/0000-0001-5675-9372

Complete contact information is available at: https://pubs.acs.org/10.1021/acs.inorgchem.6c02037

Downloaded from pubs.acs.org/inocaj/article-pdf/65/32/18639/6435106/acs.inorgchem.6c02037.pdf by UNIV DEGLI STUDI DI PARMA user on 08 September 2026

Author Contributions

The manuscript was written through contributions of all authors. All authors have given approval to the final version of the manuscript.

Funding

The funding of MIUR within the PRIN2020 project "NICE-Nature Inspired Crystal Engineering" (PRIN2020Y2CZJ2) is acknowledged. Funding from the Ministry of University and Research (MUR, Progetto Competitivo 2024, CMPT248870) is also acknowledged. This work also benefitted from the call − Missione 4 "Istruzione e Ricerca"− Componente 2 − Investimento 1.1 "Fondo per il Programma Nazionale di Ricerca e Progetti di Rilevante Interesse Nazionale (PRIN)" with projects "X4BEES" (PRIN2022-D53D23010140001) and "FLuorInated PePtidEs for Resumption (FLIPPER)" (202224KAX8). P.P.M. also acknowledges the starting grant from the University of Parma (2025-UNPRCLE-0066646).

Notes

The authors declare no competing financial interest.

■ ACKNOWLEDGMENTS

This work has benefitted from the equipment and framework of the COMP-HUB and COMP-R Initiatives, funded by the 'Departments of Excellence' program of the Italian Ministry for University and Research (MIUR, 2018−2022 and MUR, 2023−2027). The Laboratorio di Strutturistica "M. Nardelli" of the University of Parma is acknowledged for the X-ray diffraction facilities. This research benefits from the HPC (High Performance Computing) facility of the University of Parma, Italy.

■ REFERENCES

(1) James, S. L.; Adams, C. J.; Bolm, C.; Braga, D.; Collier, P.; Friščić, T.; Grepioni, F.; Harris, K. D. M.; Hyett, G.; Jones, W.; Krebs, A.; Mack, J.; Maini, L.; Orpen, A. G.; Parkin, I. P.; Shearouse, W. C.; Steed, J. W.; Waddell, D. C. Mechanochemistry: Opportunities for New and Cleaner Synthesis. *Chem. Soc. Rev.* **2012**, *41* (1), 413−447.
(2) Beyer, M. K.; Clausen-Schaumann, H. Mechanochemistry: The Mechanical Activation of Covalent Bonds. *Chem. Rev.* **2005**, *105* (8), 2921−2948.
(3) Friščić, T.; Mottillo, C.; Titi, H. M. Mechanochemistry for Synthesis. *Angew. Chem., Int. Ed.* **2020**, *59* (3), 1018−1029.
(4) Cagossi, G.; Mazzeo, P. P.; Bacchi, A.; Pelagatti, P. Comparison between Mechanochemical and Solution Synthesis of Zn and Cu Complexes Containing Pyridine and p-Halogen Substituted Benzoates. *RSC Mechanochem.* **2025**, *2* (3), 475−481.
(5) Yaghi, O. M.; O'Keeffe, M.; Ockwig, N. W.; Chae, H. K.; Eddaoudi, M.; Kim, J. Reticular Synthesis and the Design of New Materials. *Nature* **2003**, *423* (6941), 705−714.
(6) Eddaoudi, M.; Kim, J.; Rosi, N.; Vodak, D.; Wachter, J.; O'Keeffe, M.; Yaghi, O. M. Systematic Design of Pore Size and Functionality in Isoreticular MOFs and Their Application in Methane Storage. *Science* **2002**, *295* (5554), 469−472.
(7) Li, H.; Eddaoudi, M.; O'Keeffe, M.; Yaghi, O. M. Design and Synthesis of an Exceptionally Stable and Highly Porous Metal-Organic Framework. *Nature* **1999**, *402* (6759), 276−279.
(8) Furukawa, H.; Cordova, K. E.; O'Keeffe, M.; Yaghi, O. M. The Chemistry and Applications of Metal-Organic Frameworks. *Science* **2013**, *341* (6149), 1230444.
(9) Daglar, H.; Keskin, S. Recent Advances, Opportunities, and Challenges in High-Throughput Computational Screening of MOFs for Gas Separations. *Coord. Chem. Rev.* **2020**, *422*, 213470.
(10) Yuan, H.; Li, N.; Fan, W.; Cai, H.; Zhao, D. Metal-Organic Framework Based Gas Sensors. *Adv. Sci.* **2022**, *9* (6), 2104374.
(11) Bengsch, M.; Neumann, C. N. Metal-Organic Framework−Specific Catalysis. *ChemCatchem* **2025**, *17* (6), No. e202402102.
(12) Jiang, C.; Wang, X.; Ouyang, Y.; Lu, K.; Jiang, W.; Xu, H.; Wei, X.; Wang, Z.; Dai, F.; Sun, D. Recent Advances in Metal−Organic Frameworks for Gas Adsorption/Separation. *Nanoscale Adv.* **2022**, *4* (9), 2077−2089.
(13) Peng, P.; Jiang, H. Z. H.; Collins, S.; Furukawa, H.; Long, J. R.; Breunig, H. Long Duration Energy Storage Using Hydrogen in Metal−Organic Frameworks: Opportunities and Challenges. *ACS Energy Lett.* **2024**, *9* (6), 2727−2735.
(14) Nobel Prize in Chemistry 2025.*NobelPrize.Org. Nobel Prize Outreach*. 2025<https://www.nobelprize.org/prizes/chemistry/2025/summary/>
(15) Pichon, A.; Lazuen-Garay, A.; James, S. L. Solvent-Free Synthesis of a Microporous Metal−Organic Framework. *CrystEngcomm* **2006**, *8* (3), 211.
(16) Pichon, A.; James, S. L. An Array-Based Study of Reactivity under Solvent-Free Mechanochemical Conditions—Insights and Trends. *CrystEngcomm* **2008**, *10* (12), 1839.
(17) Lv, D.; Chen, Y.; Li, Y.; Shi, R.; Wu, H.; Sun, X.; Xiao, J.; Xi, H.; Xia, Q.; Li, Z. Efficient Mechanochemical Synthesis of MOF-5 for Linear Alkanes Adsorption. *J. Chem. Eng. Data* **2017**, *62* (7), 2030−2036.
(18) Užarević, K.; Wang, T. C.; Moon, S.-Y.; Fidelli, A. M.; Hupp, J. T.; Farha, O. K.; Friščić, T. Mechanochemical and Solvent-Free Assembly of Zirconium-Based Metal−Organic Frameworks. *Chem. Commun* **2016**, *52* (10), 2133−2136.
(19) Rodríguez-Sánchez, N.; Prinz, C.; Bienert, R.; Ballesteros, M.; Ruiz Salvador, A. R.; Bhattacharya, B.; Emmerling, F. Mechanochemical ZIF-9 Formation: In Situ Analysis and Photocatalytic Enhancement Evaluation. *RSC Mechanochem.* **2025**, *2* (1), 116−126.
(20) Brekalo, I.; Lisac, K.; Ramirez, J. R.; Pongrac, P.; Puškarić, A.; Valić, S.; Xu, Y.; Ferguson, M.; Marrett, J. M.; Arhangelskis, M.; Friščić, T.; Holman, K. T. Mechanochemical Solid Form Screening of Zeolitic Imidazolate Frameworks Using Structure-Directing Liquid Additives. *J. Am. Chem. Soc.* **2025**, *147* (31), 27413−27430.
(21) Katsenis, A. D.; Puškarić, A.; Štrukil, V.; Mottillo, C.; Julien, P. A.; Užarević, K.; Pham, M.-H.; Do, T.-O.; Kimber, S. A. J.; Lazić, P.; Magdysyuk, O.; Dinnebier, R. E.; Halasz, I.; Friščić, T. In Situ X-Ray Diffraction Monitoring of a Mechanochemical Reaction Reveals a Unique Topology Metal-Organic Framework. *Nat. Commun.* **2015**, *6* (1), 6662.
(22) Desai, A. V.; Sharma, S.; Let, S.; Ghosh, S. K. N-Donor Linker Based Metal-Organic Frameworks (MOFs): Advancement and Prospects as Functional Materials. *Coord. Chem. Rev.* **2019**, *395*, 146−192.
(23) ZareKarizi, F.; Joharian, M.; Morsali, A. Pillar-Layered MOFs: Functionality, Interpenetration, Flexibility and Applications. *J. Mater. Chem. A* **2018**, *6* (40), 19288−19329.
(24) Bury, W.; Fairen-Jimenez, D.; Lalonde, M. B.; Snurr, R. Q.; Farha, O. K.; Hupp, J. T. Control over Catenation in Pillared Paddlewheel Metal−Organic Framework Materials via Solvent-Assisted Linker Exchange. *Chem. Mater.* **2013**, *25* (5), 739−744.
(25) Perego, J.; Daolio, A.; Bezuidenhout, C. X.; Piva, S.; Prando, G.; Costarella, B.; Carretta, P.; Marchiò, L.; Kubicki, D.; Sozzani, P.; Bracco, S.; Comotti, A. Solid State Machinery of Multiple Dynamic Elements in a Metal−Organic Framework. *Angew. Chem., Int. Ed.* **2024**, *63* (10), No. e202317094.
(26) Balestri, D.; Costa, D.; Bacchi, A.; Carlucci, L.; Pelagatti, P. Linker Dependent Dimensionality in Zn(II)-Coordination Polymers Containing a Flexible Bis-Pyridyl-Bis-Amide Ligand. *Polyhedron* **2018**, *153*, 278−285.
(27) Chen, Y.; Wu, H.; Yuan, Y.; Lv, D.; Qiao, Z.; An, D.; Wu, X.; Liang, H.; Li, Z.; Xia, Q. Highly Rapid Mechanochemical Synthesis of a Pillar-Layer Metal-Organic Framework for Efficient CH_4/N_2 Separation. *Chem. Eng. J.* **2020**, *385*, 123836.
(28) Cagossi, G.; Piombo, B.; Daolio, A.; Mazzeo, P. P.; Bacchi, A.; Pelagatti, P. Shaping Coordination Polymers by Ball Milling. *RSC Mechanochem.* **2026**, *3*, 280.

Downloaded from pubs.acs.org/inocaj/article-pdf/65/32/18639/6643510/acs.inorgchem.6c02037.pdf by UNIV DEGLI STUDI DI PARMA user on 08 September 2026

(29) Balestri, D.; Bacchi, A.; Scilabra, P.; Pelagatti, P. Extension of the Pd-Catalyzed C−N Bond Forming Reaction to the Synthesis of Large Polydentate Ligands Containing N−H Functions. *Inorg. Chim. Acta* **2018**, *470*, 416−422.
(30) Balestri, D.; Mazzeo, P. P.; Carraro, C.; Demitri, N.; Pelagatti, P.; Bacchi, A. Stepwise Evolution of Molecular Nanoaggregates Inside the Pores of a Highly Flexible Metal−Organic Framework. *Angew. Chem., Int. Ed.* **2019**, *58* (48), 17342−17350.
(31) Balestri, D.; Mazzeo, P. P.; Perrone, R.; Fornari, F.; Bianchi, F.; Careri, M.; Bacchi, A.; Pelagatti, P. Deciphering the Supramolecular Organization of Multiple Guests Inside a Microporous MOF to Understand Their Release Profile. *Angew. Chem., Int. Ed.* **2021**, *60* (18), 10194−10202.
(32) Mazzeo, P. P.; Balestri, D.; Bacchi, A.; Pelagatti, P. Stabilization of Liquid Active Guests via Nanoconfinement into a Flexible Microporous Metal−Organic Framework. *CrystEngcomm* **2021**, *23* (41), 7262−7269.
(33) Giovanardi, D.; Cagossi, G.; Zolotarev, P. N.; Mazzeo, P. P.; Bacchi, A.; Carlucci, L.; Proserpio, D. M.; Pelagatti, P. Collapse or Capture? Guest-Induced Response of Two Structurally Distinct Pillared-MOFs upon Exposure to Pyridines and Quinolines. *Dalton Trans.* **2025**, *54* (36), 13540−13548.
(34) Daolio, A.; Giovanardi, D.; Mazzeo, P. P.; Pelagatti, P.; Bacchi, A. The Dynamic Adaptability of Mixed-Ligand Zinc MOFs: From Fundaments to Applications. *Coord. Chem. Rev.* **2026**, *553*, 217509.
(35) Fornari, F.; Bianchi, F.; Riboni, N.; Casoli, F.; Bacchi, A.; Mazzeo, P. P.; Pelagatti, P.; Careri, M. Metal-Organic Framework-Based Magnetic Dispersive Micro-Solid-Phase Extraction for the Gas Chromatography−Mass Spectrometry Determination of Polycyclic Aromatic Compounds in Water Samples. *J. Chromatogr. A* **2022**, *1671*, 463010.
(36) Portolés-Gil, N.; Lanza, A.; Aliaga-Alcalde, N.; Ayllón, J. A.; Gemmi, M.; Mugnaioli, E.; López-Periago, A. M.; Domingo, C. Crystalline Curcumin bioMOF Obtained by Precipitation in Supercritical CO_2 and Structural Determination by Electron Diffraction Tomography. *ACS Sustainable Chem. Eng.* **2018**, *6* (9), 12309−12319.
(37) Cichocka, M. O.; Liang, Z.; Feng, D.; Back, S.; Siahrostami, S.; Wang, X.; Samperisi, L.; Sun, Y.; Xu, H.; Hedin, N.; Zheng, H.; Zou, X.; Zhou, H.-C.; Huang, Z. A Porphyrinic Zirconium Metal−Organic Framework for Oxygen Reduction Reaction: Tailoring the Spacing between Active-Sites through Chain-Based Inorganic Building Units. *J. Am. Chem. Soc.* **2020**, *142* (36), 15386−15395.
(38) Lenzen, D.; Zhao, J.; Ernst, S.-J.; Wahiduzzaman, M.; Ken Inge, A.; Fröhlich, D.; Xu, H.; Bart, H.-J.; Janiak, C.; Henninger, S.; Maurin, G.; Zou, X.; Stock, N. A Metal−Organic Framework for Efficient Water-Based Ultra-Low-Temperature-Driven Cooling. *Nat. Commun.* **2019**, *10* (1), 3025.
(39) Faye Diouf, M. D.; Marchetti, D.; Parlanti, P.; Pedrini, A.; Gemmi, M. Automated Serial Electron Diffraction: Implementation in LibraEDT and Its Applications. *J. Appl. Crystallogr.* **2026**, *59* (3), 858−868.
(40) Sala, A.; Faye Diouf, M. D.; Marchetti, D.; Pasquale, L.; Gemmi, M. Mechanochemical Synthesis and Three-Dimensional Electron Diffraction Structure Solution of a Novel Cu-Based Protocatechuate Metal−Organic Framework. *Cryst. Growth Des.* **2024**, *24* (8), 3246−3255.
(41) Marchetti, D.; Riboni, N.; Inge, A. K.; Cheung, O.; Gemmi, M.; Dalcanale, E.; Bianchi, F.; Massera, C.; Pedrini, A. A Flexible Interpenetrated Diamondoid Metal−Organic Framework with Aromatic-Enriched Channels as a Preconcentrator for the Detection of Fluorinated Anesthetics. *Chem. Mater.* **2025**, *37* (6), 2230−2240.
(42) Sabena, C.; Bravetti, F.; Miyauchi, N.; Nakafukasako, M.; Aoyama, Y.; Asakura, K.; Konuma, K.; Hashimoto, M.; Nishiyama, Y.; Chierotti, M. R. An Integrated Workflow for the Structure Elucidation of Nanocrystalline Powders. *Commun. Chem.* **2026**, *9* (1), 97.
(43) Dubskikh, V. A.; Lysova, A. A.; Samsonenko, D. G.; Dybtsev, D. N.; Fedin, V. P. Topological Polymorphism and Temperature-Driven Topotactic Transitions of Metal−Organic Coordination Polymers. *CrystEngcomm* **2020**, *22* (38), 6295−6301.
(44) Matemb Ma Ntep, T. J.; Wahiduzzaman, M.; Laurenz, E.; Cornu, I.; Mouchaham, G.; Dovgaliuk, I.; Nandi, S.; Knop, K.; Jansen, C.; Nouar, F.; Florian, P.; Füldner, G.; Maurin, G.; Janiak, C.; Serre, C. When Polymorphism in Metal−Organic Frameworks Enables Water Sorption Profile Tunability for Enhancing Heat Allocation and Water Harvesting Performance. *Adv. Mater.* **2024**, *36* (12), 2211302.
(45) Mendes, N. P. D. A.; Souto Neto, A. L. D.; Hortêncio, J. D. S.; Menezes De Oliveira, A. L.; Raimundo, R. A.; Macedo, D. A.; Da Silva, F. F. Impact of the Metal−Organic Frameworks Polymorphism on the Electrocatalytic Properties of CeO_2 toward Oxygen Evolution. *ACS Omega* **2024**, *9* (50), 49913−49924.
(46) Aulakh, D.; Varghese, J. R.; Wriedt, M. The Importance of Polymorphism in Metal−Organic Framework Studies. *Inorg. Chem.* **2015**, *54* (17), 8679−8684.
(47) Chaemchuen, S.; Zhou, K.; Yusubov, M. S.; Postnikov, P. S.; Klomkliang, N.; Verpoort, F. Solid-State Transformation in Porous Metal-Organic Frameworks Based on Polymorphic-Pillared Net Structure: Generation of Tubular Shaped MOFs. *Microporous Mesoporous Mater.* **2019**, *278*, 99−104.
(48) Zhu, N.; Lennox, M. J.; Düren, T.; Schmitt, W. Polymorphism of Metal−Organic Frameworks: Direct Comparison of Structures and Theoretical N_2 -Uptake of Topological Pto- and Tbo-Isomers. *Chem. Commun.* **2014**, *50* (32), 4207−4210.
(49) Braga, D.; Maini, L.; Mazzeo, P. P.; Ventura, B. Reversible Interconversion between Luminescent Isomeric Metal−Organic Frameworks of $[Cu_4I_4(DABCO)_2]$(DABCO=1,4-Diazabicyclo-[2.2.2]octane). *Chem. − Eur. J.* **2010**, *16* (5), 1553−1559.
(50) Balestri, D.; Scilabra, P.; Carraro, C.; Delledonne, A.; Bacchi, A.; Mazzeo, P. P.; Carlucci, L.; Pelagatti, P. Structural, Thermal and Topological Characterization of Coordination Networks Containing Flexible Aminocarboxylate Ligands with a Central Biphenylene Scaffold. *CrystEngcomm* **2019**, *21* (42), 6365−6373.
(51) Shivanna, M.; Yang, Q.-Y.; Bajpai, A.; Patyk-Kazmierczak, E.; Zaworotko, M. J. A Dynamic and Multi-Responsive Porous Flexible Metal−Organic Material. *Nat. Commun.* **2018**, *9* (1), 3080.
(52) Seo, J.; Bonneau, C.; Matsuda, R.; Takata, M.; Kitagawa, S. Soft Secondary Building Unit: Dynamic Bond Rearrangement on Multinuclear Core of Porous Coordination Polymers in Gas Media. *J. Am. Chem. Soc.* **2011**, *133* (23), 9005−9013.
(53) Karadeniz, B.; Žilić, D.; Huskić, I.; Germann, L. S.; Fidelli, A. M.; Muratović, S.; Lončarić, I.; Etter, M.; Dinnebier, R. E.; Barišić, D.; Cindro, N.; Islamoglu, T.; Farha, O. K.; Friščić, T.; Užarević, K. Controlling the Polymorphism and Topology Transformation in Porphyrinic Zirconium Metal−Organic Frameworks via Mechanochemistry. *J. Am. Chem. Soc.* **2019**, *141* (49), 19214−19220.
(54) Eubank, J. F.; Wojtas, L.; Hight, M. R.; Bousquet, T.; Kravtsov, V. C.; Eddaoudi, M. The Next Chapter in MOF Pillaring Strategies: Trigonal Heterofunctional Ligands To Access Targeted High-Connected Three Dimensional Nets, Isoreticular Platforms. *J. Am. Chem. Soc.* **2011**, *133* (44), 17532−17535.
(55) Giovanardi, D.; Mazzeo, P. P.; Pelagatti, P.; Bacchi, A. Guest Molecules Play Tug of War in a Breathing MOF: The Stepwise Monitoring of an Elastic Framework Deformation via SC-SC Transformations. *Cryst. Growth Des.* **2023**, *23* (12), 8726−8734.
(56) Coelho, A. A. TOPAS and TOPAS-Academic: An Optimization Program Integrating Computer Algebra and Crystallographic Objects Written in C++. *J. Appl. Crystallogr.* **2018**, *51* (1), 210−218.
(57) Gemmi, M.; Mugnaioli, E.; Gorelik, T. E.; Kolb, U.; Palatinus, L.; Boullay, P.; Hovmöller, S.; Abrahams, J. P. 3D Electron Diffraction: The Nanocrystallography Revolution. *ACS Cent. Sci.* **2019**, *5* (8), 1315−1329.
(58) Lanza, A.; Margheritis, E.; Mugnaioli, E.; Cappello, V.; Garau, G.; Gemmi, M. Nanobeam Precession-Assisted 3D Electron Diffraction Reveals a New Polymorph of Hen Egg-White Lysozyme. *IUCrJ.* **2019**, *6* (2), 178−188.
(59) Mugnaioli, E.; Gorelik, T.; Kolb, U. "Ab Initio" Structure Solution from Electron Diffraction Data Obtained by a Combination of Automated Diffraction Tomography and Precession Technique. *Ultramicroscopy* **2009**, *109* (6), 758−765.

Downloaded from pubs.acs.org/inocaj/article-pdf/65/32/18639/6435106/acs.inorgchem.6c02037.pdf by UNIV DEGLI STUDI DI PARMA user on 08 September 2026

(60) Palatinus, L.; Brázda, P.; Jelínek, M.; Hrdá, J.; Steciuk, G.; Klementová, M. Specifics of the Data Processing of Precession Electron Diffraction Tomography Data and Their Implementation in the Program PETS2.0. *Acta Crystallogr., Sect. B: Struct. Sci., Cryst. Eng. Mater.* **2019**, *75* (4), 512−522.
(61) Burla, M. C.; Caliandro, R.; Carrozzini, B.; Cascarano, G. L.; Cuocci, C.; Giacovazzo, C.; Mallamo, M.; Mazzone, A.; Polidori, G. Crystal Structure Determination and Refinement via SIR2014. *J. Appl. Crystallogr.* **2015**, *48* (1), 306−309.
(62) Zhang, Y.-B.; Su, J.; Furukawa, H.; Yun, Y.; Gándara, F.; Duong, A.; Zou, X.; Yaghi, O. M. Single-Crystal Structure of a Covalent Organic Framework. *J. Am. Chem. Soc.* **2013**, *135* (44), 16336−16339.
(63) Romagnoli, L.; D'Annibale, A.; Blundo, E.; Patra, A.; Polimeni, A.; Meggiolaro, D.; Andrusenko, I.; Marchetti, D.; Gemmi, M.; Latini, A. 4,4′-(Anthracene-9,10-Diylbis(Ethyne-2,1-Diyl))Bis(1-Methyl-1-Pyridinium) Lead Iodide $C_{30}H_{22}N_2Pb_2I_6$: A Highly Luminescent, Chemically and Thermally Stable One-Dimensional Hybrid Iodoplumbate. *Chem. Mater.* **2023**, *35* (4), 1818−1826.
(64) Das, P. P.; Mugnaioli, E.; Nicolopoulos, S.; Tossi, C.; Gemmi, M.; Galanis, A.; Borodi, G.; Pop, M. M. Crystal Structures of Two Important Pharmaceuticals Solved by 3D Precession Electron Diffraction Tomography. *Org. Process Res. Dev.* **2018**, *22* (10), 1365−1372.
(65) Andrusenko, I.; Hamilton, V.; Lanza, A. E.; Hall, C. L.; Mugnaioli, E.; Potticary, J.; Buanz, A.; Gaisford, S.; Piras, A. M.; Zambito, Y.; Hall, S. R.; Gemmi, M. Structure Determination, Thermal Stability and Dissolution Rate of δ-Indomethacin. *Int. J. Pharm.* **2021**, *608*, 121067.
(66) Dassault Systèmes. *BIOVIA Materials Studio (Versione 2023)*; Dassault Systèmes BIOVIA, 2023.
(67) Clark, S. J.; Segall, M. D.; Pickard, C. J.; Hasnip, P. J.; Probert, M. I. J.; Refson, K.; Payne, M. C. First Principles Methods Using CASTEP. *Z. Für Krist. - Cryst. Mater.* **2005**, *220* (5−6), 567−570.
(68) El-Sayed, D. S. Electronic Band Structure and Density of State Modulation of Amphetamine and ABW Type−Zeolite Adsorption System: DFT-CASTEP Analysis. *J. Mol. Model.* **2023**, *29* (4), 96.
(69) Wang, Y.; Li, M.; Duanmu, P.; Yang, H.; Yuan, H.; Li, X. Mechanisms of Curcumin Adsorption in Metal-Substituted MOF-74 Frameworks Using DFT and MD Simulations. *Sci. Rep.* **2026**, *16* (1), 263.
(70) Perego, J.; Bezuidenhout, C. X.; Bracco, S.; Piva, S.; Prando, G.; Aloisi, C.; Carretta, P.; Kaleta, J.; Le, T. P.; Sozzani, P.; Daolio, A.; Comotti, A. Benchmark Dynamics of Dipolar Molecular Rotors in Fluorinated Metal-Organic Frameworks. *Angew. Chem., Int. Ed.* **2023**, *62* (5), No. e202215893.
(71) Adamo, C.; Barone, V. Toward Reliable Density Functional Methods without Adjustable Parameters: The PBE0Model. *J. Chem. Phys.* **1999**, *110* (13), 6158−6170.
(72) Tkatchenko, A.; Scheffler, M. Accurate Molecular Van Der Waals Interactions from Ground-State Electron Density and Free-Atom Reference Data. *Phys. Rev. Lett.* **2009**, *102* (7), 073005.
(73) Blatov, V. A.; Shevchenko, A. P.; Proserpio, D. M. Applied Topological Analysis of Crystal Structures with the Program Package ToposPro. *Cryst. Growth Des.* **2014**, *14* (7), 3576−3586.
(74) Shevchenko, A. P.; Shabalin, A. A.; Karpukhin, I. Y.; Blatov, V. A. Topological Representations of Crystal Structures: Generation, Analysis and Implementation in the TopCryst System. *Sci. Technol. Adv. Mater.: Methods* **2022**, *2* (1), 250−265.
(75) Wang, Z.; Li, Z.; Ng, M.; Milner, P. J. Rapid Mechanochemical Synthesis of Metal−Organic Frameworks Using Exogenous Organic Base. *Dalton Trans.* **2020**, *49* (45), 16238−16244.
(76) Blatov, V. A.; Proserpio, D. M. Topological Relations between Three-Periodic Nets. II. Binodal Nets. *Acta Crystallogr., Sect. A* **2009**, *65* (3), 202−212.
(77) CCDC2541762 contains the supplementary crystallographic data for this paper. These data are provided free of charge by the joint Cambridge Crystallographic Data Centre and Fachinformationszentrum Karlsruhe Access Structures service www.ccdc.cam.ac.uk/structures
(78) Cao, J.; Ma, W.; Lyu, K.; Zhuang, L.; Cong, H.; Deng, H. Twist and Sliding Dynamics between Interpenetrated Frames in Ti-MOF Revealing High Proton Conductivity. *Chem. Sci.* **2020**, *11* (15), 3978−3985.
(79) Senkovska, I.; Bon, V.; Abylgazina, L.; Mendt, M.; Berger, J.; Kieslich, G.; Petkov, P.; Luiz Fiorio, J.; Joswig, J.-O.; Heine, T.; Schaper, L.; Bachetzky, C.; Schmid, R.; Fischer, R. A.; Pöppl, A.; Brunner, E.; Kaskel, S. Understanding MOF Flexibility: An Analysis Focused on Pillared Layer MOFs as a Model System. *Angew. Chem., Int. Ed.* **2023**, *62* (33), No. e202218076.

Downloaded from pubs.acs.org/inocaj/article-pdf/65/32/18639/6643510 6/acs.inorgchem.6c02037.pdf by UNIV DEGLI STUDI DI PARMA user on 08 September 2026

https://doi.org/10.1021/acs.inorgchem.6c02037
Inorg. Chem. 2026, 65, 18639−18647